NUCL SCI TECH (2019) 30:51
https://doi.org/10.1007/s41365-019-0574-6

Design and flow field analysis for visualization experiment facility of pebble bed based on molten salt reactor

Mu-Dan Mei[1,2] · Xing-Wei Chen[1,2] · Sheng-De Sun[1,2] · Rui Yan[1,2] · Yang Zou[1,2]

Received: 2 February 2018 / Revised: 31 August 2018 / Accepted: 9 September 2018 / Published online: 20 February 2019

Abstract Molten salt pebble bed reactor is one of the sixth-generation IV reactor types. To investigate the mechanical behavior of the fuel pebbles in the core, a visualization experiment facility of pebble bed (VEFPB) is designed. To obtain a uniform flow field of the core and analyze the influence of the flow field on the structure of the pebble bed, computational fluid dynamics software Fluent is used to simulate the flow field distribution of the core of VEFPB. The simulation results show that the disturbance at the bottom of the pebble bed is proportional to the flow velocity of the inlet pipe, and the flow velocity close to the inlet side is more significant than that in other parts; the design of the cylinder bottom plate with holes of different sizes can effectively reduce the flow velocity and the disturbance at the bottom of the pebble bed. In addition, according to the velocity contours of the core of VEFPB, it is observed that the flow field distribution of the core is considerably uniform except at the bottom of the pebble bed. This ensures the stability of the pebble bed and verifies the rationality of the design of VEFPB. This study provides the technical support and reference for the flow field analysis of the core of molten salt pebble bed reactor.

This work was supported by the Strategic Priority Research Program of the Chinese Academy of Sciences (No. XD02010000) and the Frontier Science Key Program of the Chinese Academy of Sciences (No. QYZDY-SSW-JSC016).

✉ Yang Zou
zouyamg@sinap.ac.cn

1 Shanghai Institute of Applied Physics, Chinese Academy of Sciences, Shanghai 201800, China

2 University of Chinese Academy of Sciences, Beijing 100049, China

Keywords Thorium molten salt reactor (TMSR) · Particle image velocimetry (PIV) · Computational fluid dynamics (CFD) · Experiment facility

1 Introduction

Thorium molten salt reactor (TMSR) is a high-temperature fluoride salt-cooled pebble bed reactor, with the fuel pebbles packing randomly in the core to form a random pebble bed. TMSR is a new type of reactor, and there are few studies about the stacking behavior of the pebble bed in molten salt, both in China and in abroad [1–5]. Therefore, a visualization experiment facility of pebble bed (VEFPB) is designed, and its size is half the TMSR device; it uses particle image velocimetry (PIV) and allows for fully three-dimensional imaging and tracking of particles in a densely packed pebble bed. The PIV instrument is based on the matching index scan method, and the bulk is visible when immersing transparent particles in a fluid with the same index of refraction; we acquire the stacking behavior of the pebble bed of the whole core of VEFPB by image acquisition and pebble bed refactoring, finally to provide the basis for the research on the pebble bed stacking sequence of TMSR, such as the bulk density and the distribution rule of the pebble bed [6, 7].

As the stability of stacking structure of fuel spheres in the core is one of the indicators of stable and safe operation of the reactor system, it is necessary to perform numerical simulation and maintain the flow field of the core of VEFPB uniform. Through the simulation of the flow field, we can more accurately observe, monitor, and analyze the movement characteristics of the internal fluid in VEFPB, including the fluid at the bottom of the pebble bed, the fluid in the molten salt channels of the reflector, etc.

During the study, we design the VEFPB based on the results of modeling analysis [8]. Meanwhile, considering the 1:1 model of VEFPB as a research object, we simulate the flow field distribution of the core of VEFPB. The results of the flow field analysis verify the feasibility and rationality of the design of VEFPB preliminarily.

2 Methods

2.1 Design of visualization experimental facility of pebble bed

The purpose of the design of VEFPB is to acquire three-dimensional imaging and obtain the tracking of particles in a densely packed pebble bed. The VEFPB consists of a hydraulic circuit system, simulation core system, PIV test system, and logic control system. The simulation core system mainly includes the main container, sphere storage tank, sphere feed mechanism, and sphere discharging mechanism and is shown in Fig. 1. The main container consists of an external square container and an internal cylindrical simulation core container. The flow field analysis of VEFPB is performed to study the fluid movement characteristic of the core, with the simulation core container of VEFPB as the research object, and mainly gives its design. VEFPB comprises the core, fluid inlet and outlet pipes, fuel sphere inlet and outlet pipes, flow distribution plate, upper and lower reflectors, inner and outer cylinders of the core, core shroud floor, upper and lower ring chambers, and upper and lower cover plates of the outer cylinder. The schematic of VEFPB is shown in Fig. 2. The gap between the inner and outer cylinders of the core constitutes the downtrend ring cavity.

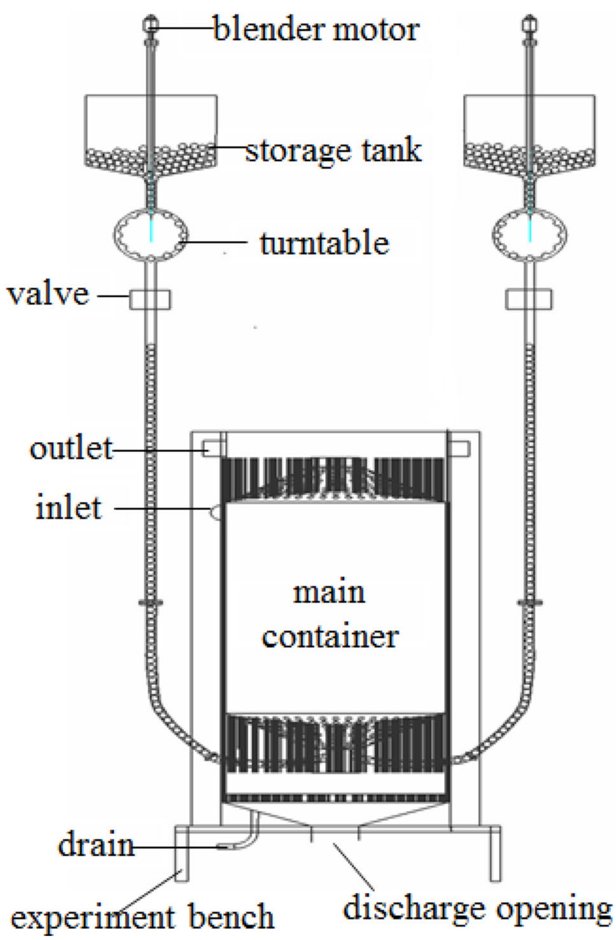

Fig. 1 Schematic of the simulation core system of VEFPB

VEFPB uses a plastic ball made of polymethyl methacrylate (PMMA) to simulate the fuel sphere of TMSR and sodium iodide solution as the fluid. The temperature of the fluid inlet and outlet is 20 °C, and the inlet pipe slant has a tangential angle of 30° on the outer cylinder of the core. Sodium iodide solution first runs into the downtrend ring cavity through the inlet pipe, then into the lower ring chamber through the flow distribution plate, then up into the core shroud floor and the molten salt channels of the lower reflector, and finally flows into the core of VEFPB, the upper reflector, the upper ring chamber, and the outlet pipe in turn. The sphere inlet pipes located at the bottom of the main container are symmetrical.

The design of main components of the simulation core container based on the hydraulic equivalent analysis method is shown in Fig. 3 [9, 10].

The inlet pipe and the outlet pipe are shown in Fig. 3a. The molten salt from the upper ring chamber runs up to two symmetrical pipes and then converges to the outlet pipe. The flow distribution plate has 576 holes with Φ 12.5 mm

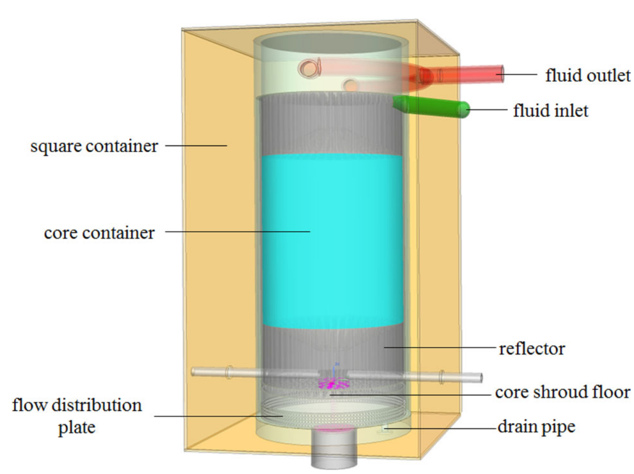

Fig. 2 (Color online) Three-dimensional diagram of the main container of VEFPB

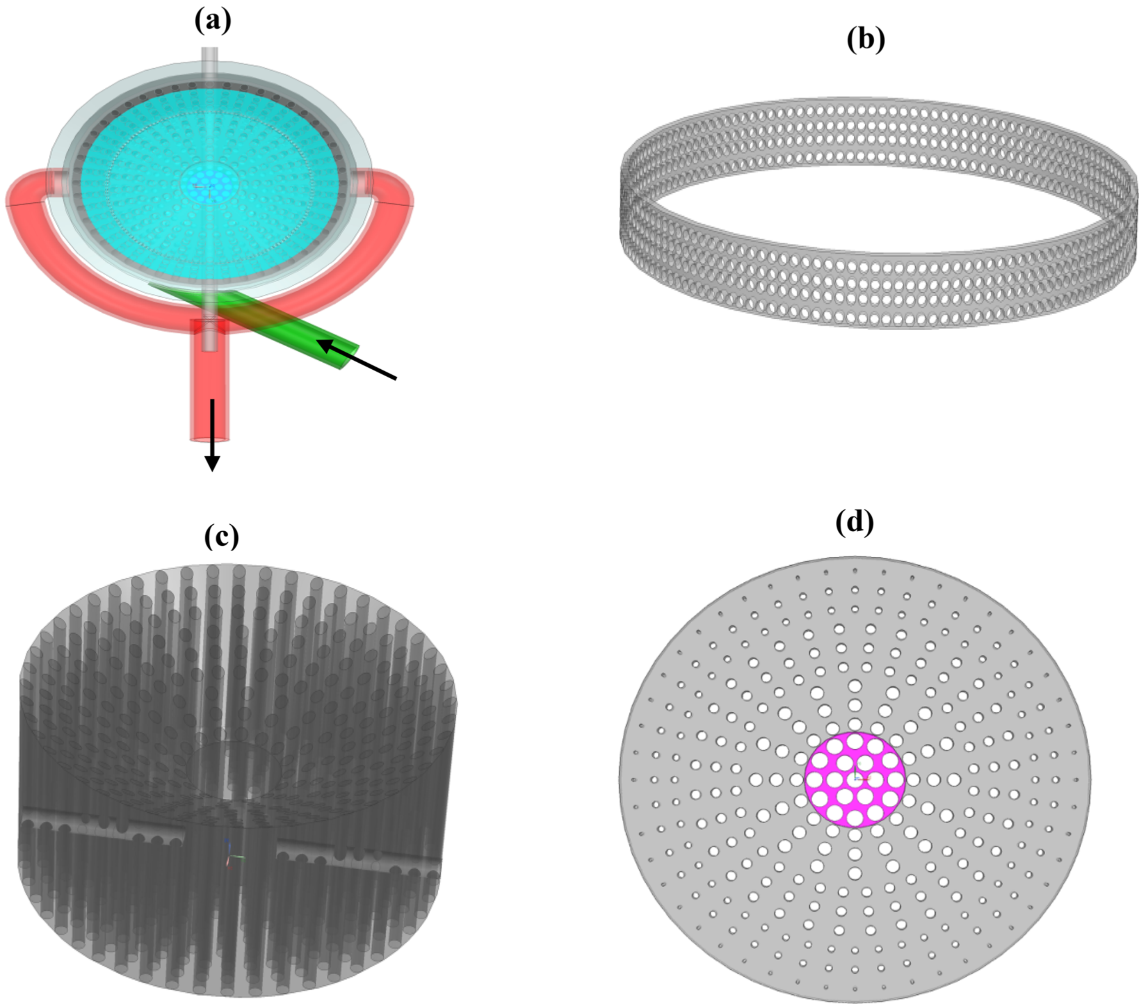

Fig. 3 (Color online) Structure of main components of the simulation core of VEFPB: **a** Inlet and outlet pipes, **b** flow distribution plate, **c** axial reflector, and **d** core shroud floor

that are arranged in four rings evenly. This design can effectively reduce the velocity of molten salt from the downtrend ring cavity. The upper (lower) reflector has 288 molten salt channels and has a through hole with *Φ* 150 mm in the middle. The diameter of all molten salt channels is 20 mm, and these channels are uniformly distributed in circumferential direction, and the through hole connects with the two sphere inlet pipes. The core shroud floor has 307 molten salt channels and a central circle, and those are independent of each other. The 307 channels align with the lower reflector, with the diameters of channels are 25, 20, 15, 10, and 5 mm from the center to the edge, respectively, to obtain a uniform flow field in the core as far as possible. The central circle with *Φ* 150 mm has 19 channels with *Φ* 25 mm.

3 Flow field analysis of the core of VEFPB

3.1 Geometric model

To simplify the simulation analysis, the external square container was omitted when building the geometric model of VEFPB because it has no effect on the core flow field, and only the internal cylindrical simulation core container was considered [11–13]. The fluid outlet pipe and the two symmetrical pipes connected with the upper ring chamber are all belong to the outlet of VEFPB, the flow field of these positions also has no impact on the flow field analysis of the core, and the two symmetrical pipes are directly simplified as the outlets in the flow field analysis of VEFPB.

The following are the design parameters of VEFPB. The total height of the simulation core container is 2115 mm. Besides, the inside and outside diameter of the outer cylinder of the core is 725 mm and 745 mm, and the inside and outside diameter of the inner cylinder of the core is 675 mm and 695 mm. The height of the core with Φ 675 mm is 900 mm, and the heights of the upper and lower reflectors are all 316 mm. The heights of the core shroud and the flow distribution plate are all 75 mm, and the heights of the core shroud floor and the upper ring chamber are 40 mm and 300 mm. Based on the above model simplification, we used 3D modeling software called Unigraphics NX (UG8.0) to build the model. Finally, the established and simplified geometric model of VEFPB is shown in Fig. 4.

3.2 Meshing

The simplified geometric model of VEFPB is imported to GAMBIT, which is the preprocessing software used in CFD analysis, and the fluid computational domain is determined according to the fluid motion path of the simulation core container. The fluid computational domain contains the inlet pipe, downtrend ring cavity, channels of the flow distribution plate, lower ring chamber, channels of the core shroud floor and the lower reflector, core of VEFPB, channels of the upper reflector, upper ring chamber, and two symmetrical outlet pipes.

The automatic grid generation method uses an unstructured grid for each fluid computational domain of VEFPB [14, 15]. As the torsion angle at the interface of the inlet and the downtrend ring cavity is larger, and the change of the flow field is obvious, this interface is meshed by selecting “Tri” as Elements and “Pave” as Type, and the inlet pipe is meshed with “Tet/Hybrid” as Elements. Meanwhile, the channels of the flow distribution plate, channels of the core shroud floor, and channels of the lower reflector are all have obvious flow field changes; thus, these channels will use the local mesh encryption method. This means that first the faces of these channels are meshed with a small internal size, and then, the body of these channels is meshed [16, 17].

The diameters of channels of the core shroud floor from the center to the edge are inconsistent; take the mesh generation of channels of the core shroud floor, for example [18]. First, the mesh for the undersurfaces of channels of the core shroud floor is refined. Select “Quad” as Elements and “Pave” as Type, and set up “internal size” with 1 for the undersurfaces of the channels with Φ 5 mm; but for the undersurfaces of the channels with Φ 10 mm and Φ 15 mm, the “internal size” of grid is set to 1.5, and for the other undersurfaces of the channels, the “internal size” is set to 2. The grid about a quarter of the undersurfaces of channels of the core shroud floor is shown in Fig. 5. Secondly, because all of the channels are regular cylinders, the channels of the core shroud floor are meshed with “Hex/Wedge” as Elements and with “Copper” as Type, and the “internal size” of the grid is set to 2. The body grid of channels of the core shroud floor is shown in Fig. 6.

3.3 Sensitivity analysis of grid

The whole fluid computational domain is divided into disparate regions for different scales of structures. According to the geometric characteristics of the model

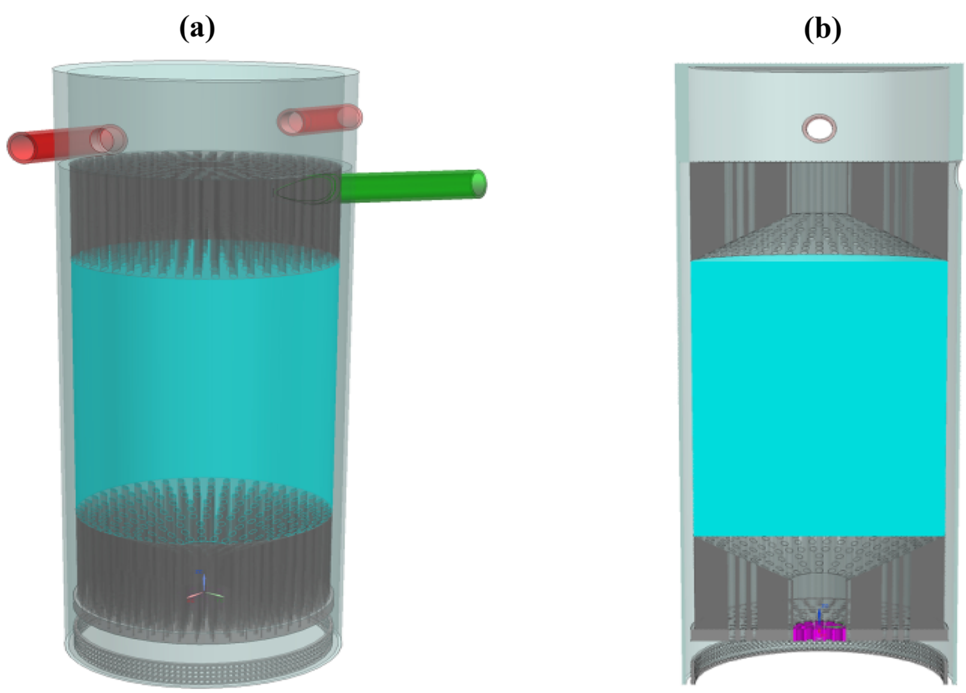

Fig. 4 (Color online) Geometric model of simplified VEFPB: **a** Three-dimensional diagram and **b** profile map

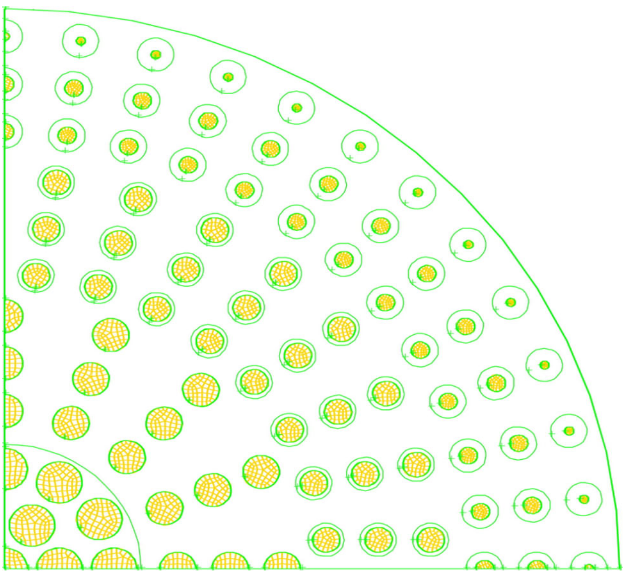

Fig. 5 Grid about a quarter of the undersurfaces of channels of the core shroud floor

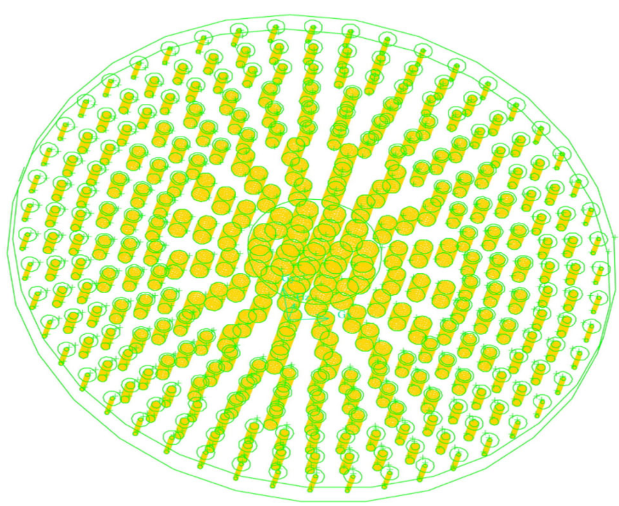

Fig. 6 (Color online) Meshing of the core shroud floor

and meshing experience, the regions with channels are meshed with small scales for their small structures and the other regions can be meshed with larger scales [19–22]. When the mass flow rate is equal to 23.7 kg/s, the sensitivities of the grid are analyzed under the condition of the core with the flow distribution plate and the core shroud floor. First, keep the same grid spaces of the undersurfaces of channels of the core shroud floor, such as the grid space equal to 1 mm in the undersurfaces of channels with Φ 5 mm, grid space equal to 1.5 mm in the undersurfaces of channels with Φ 10 mm and Φ 15 mm, and grid space equal to 3 mm in other undersurfaces of channels. Secondly, two different uniform grid systems as grid space equal to 1 mm, 2 mm in channels that contain the inlet and outlet, channels of the flow distribution plate, channels of the core shroud floor, channels of the upper and lower reflector and grid space equal to 3 mm, 6 mm in other calculation regions are investigated to validate the solution independency of the grid number. The maximum velocity in the core for the two different grid systems is listed in Table 1.

From the table, it can be seen that no clear distinction exists among the maximum velocity obtained from the two different body grid systems. Therefore, each of them can be regarded as grid independent, and the grid space equal to 2 mm in channels and grid space equal to 6 mm in other calculation regions are adopted as the final grid system considering the CPU time.

In addition, the grid space of all channels and the other calculation regions is kept constant to validate the independency of the grid number, with the same sensitivity analysis method for the undersurfaces of channels of the core shroud floor; it means that use two different grid sizes as grid space equal to 1 mm, 1.5 mm, 2 mm, and 0.5 mm, 1 mm, 2 mm in the undersurfaces of channels, for example, the undersurfaces of channels with Φ 5 mm are meshed with grid sizes as grid space equal to 1 mm or 0.5 mm, the undersurfaces of channels with Φ 10 mm and Φ 15 mm are meshed with grid sizes as grid space equal to 1.5 mm or 1 mm, and the undersurfaces of channels with Φ 20 mm and Φ 25 mm are meshed with grid sizes as grid space equal to 2 mm. The maximum velocity in the core for the two different grid sizes of the undersurfaces of channels is listed in Table 2 [23, 24].

Table 2 shows that the results for the two different grid sizes are almost consistent. Thus, the grid sizes with the grid space equal to 1 mm in the undersurfaces of channels with Φ 5 mm, the grid sizes with the grid space equal to 1.5 mm in the undersurfaces of channels with Φ 10 mm and Φ 15 mm, the grid sizes with the grid space equal to 2 mm in the undersurfaces of channels with Φ 20 mm and Φ 25 mm are regarded as grid independent and are adopted as the final grid system for the undersurfaces of channels of the core shroud floor.

3.4 Mathematical model and boundary conditions

Sodium iodide solution as the flowing medium of VEFPB has the same refractive index as the fuel spheres,

Table 1 Maximum velocity of the core with various grid spaces

Grid space (cm)	1 × 3	1 × 6	2 × 3	2 × 6
Maximum velocity (m s^{-1})	0.0369	0.037	0.0369	0.0371

Table 2 Maximum velocity of the core with various grid spaces

Grid space (cm)	1 × 1.5 × 2	0.5 × 1.5 × 2	1 × 1 × 2	0.5 × 1 × 2
Maximum velocity (m s^{-1})	0.037	0.0371	0.037	0.0369

Table 3 Physical properties of sodium iodide solution

Density (kg/m^3)	1800
Dynamic viscosity (Pa s)	0.00640

and the physical properties of this medium are shown in Table 3.

There is no decisive difference between water and sodium iodide solution from the flow viewpoint, and the mass, momentum, and energy conservation equations can also be used in sodium iodide solution. The liquid flow will be disturbed when sodium iodide solution flows through the channels and the inlet *Re* number corresponding to the inlet velocity mentioned in this paper is higher than 10,000, and is considered as turbulent flow [19]. Besides, the fluid flow is incompressible and unsteady, and the fluid–solid heat transfer and internal heat source do not need to be considered in the analysis. Therefore, the RNG turbulent model is adopted in this study, and the second-order upwind scheme SIMPLEC algorithm is used to simulate the flow field in the core of VEFPB for ensuring the accuracy of solution and convergence stability [25, 26].

The boundary conditions for the numerical simulation of VEFPB are shown in Table 4 [27, 28]. The whole fluid computational domain is divided into the fluid region and the porous zone. As the core of VEFPB is the regular packed bed, and the core consists of the pebble bed and the sodium iodide solution, it can be considered as a fluid flow filled with medium (pebble); thus, the core region of VEFPB meets the definition of a porous model, which can be defined as the porous zone in simulation. The fuel spheres with Φ 3 cm in the core are simplified as the porous medium model, and the porosity is 0.4. The viscous resistance coefficient (C_1) and the inertial resistance coefficient (C_2) of this model are acquired from Eqs. (1) and (2), which are the computational formulas of random pebble bed.

Table 4 Boundary conditions

Name	Boundary conditions
Mass flow inlet (kg s^{-1})	23.7
Inlet diameter (mm)	75
Inlet temperature (°C)	20
Reynolds number	62859
Turbulence model	RNG $k-\varepsilon$ model
Inlet turbulence intensity (%)	3.86
Hydraulic diameter (mm)	75
Pressure outlet (Pa)	101325
Gravity (m s^{-2})	− 9.817
Outlet turbulence intensity (%)	5
Outlet temperature (°C)	20
Reference pressure (Pa)	101325

$$C_1 = \frac{1}{\alpha} = \frac{180}{D_P^2}\frac{(1-\varepsilon)^2}{\varepsilon^3} = 1125000 \quad (1)$$

$$C_2 = C_F = \frac{3.834}{D_P}\frac{(1-\varepsilon)}{\varepsilon^3} = 1198.125 \quad (2)$$

D_p is the average diameter of the particles and ε and is porosity.

4 Results and discussion

The effect of the design scheme of VEFPB on the thermal hydraulics characteristics of the core in normal operation conditions with the average salt velocity of 23.7 kg/s was analyzed with Fluent software. The thermal hydraulics behaviors of VEFPB were simulated, and the main simulation results are presented here. Firstly, the flow field distribution of the core was studied, and then, the velocity distribution was analyzed in different positions of VEFPB, such as the undersurfaces of channels of the core shroud floor and the lower reflector and at the bottom of the pebble bed in the core. Thus, we can assess the influence of the design scheme of VEFPB on the velocity field in the core by analyzing the simulation results. The inlet boundary condition is constant nominal mass flow rate, and the outlet boundary condition is outflow. The velocity field and the vector distribution of the reactor core are shown in Figs. 7 and 8; the velocity field of the undersurfaces of channels of the core shroud floor and the lower reflector is shown in Figs. 9 and 10; and the velocity field at the bottom of the pebble bed in the core is shown in Fig. 11. The flow field of the upper reflector and the upper ring chamber was not analyzed because it has no influence on the flow field distribution of the pebble bed.

The calculated velocity field of the core of VEFPB is shown in Fig. 7; the field distribution of the whole core is

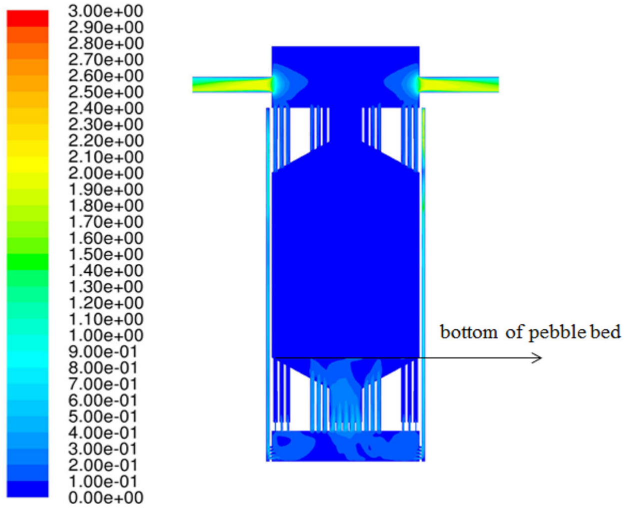

Fig. 7 (Color online) Contours of velocity distribution (m/s) of profile map of VEFPB

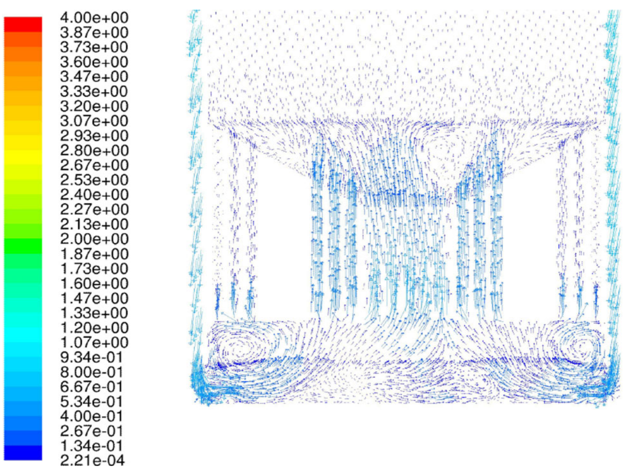

Fig. 8 (Color online) Vectors of velocity distribution (m/s) near the bottom of the core

practically stable and uniform except for the velocity field near the surface of the lower reflector, and the flow velocity in the lower ring chamber near the side of the inlet is obviously larger than the other positions of the lower ring chamber. From Fig. 8, it can be clearly seen that the vector distribution at the bottom of the core has only some small eddies near the surface of channels of the lower reflector, and that the lower ring chamber has larger eddies. The flow velocity in the channels near the center of the core shroud floor and the lower reflector is larger according to Figs. 9 and 10. Figure 11 shows that the flow field distribution at the bottom of the pebble bed in the core is almost symmetrical—only a small region has an irregular flow field in the center of the pebble bed at the bottom in the core, and the maximum flow velocity in this region is 0.105 m/s.

Figures 7, 8, 9, 10 and 11 are all discussed here, and they show that the flow field distribution of different important areas from VEFPB is more uniform and stable when the inlet velocity is less than or equal to 23.7 kg/s. Due to the limited space and the experimental requirements, the flow field of the core will not be analyzed in this work when the inlet velocity is larger than 23.7 kg/s.

The inlet velocity is 2.98 m/s acquired through unit conversion depending on the inlet mass flow of 23.7 kg/s and the fluid density and the inlet pipe diameter, and the calculations of the average velocity and the maximum velocity of the important fluid domains are shown in Table 5.

Table 5 shows that the maximum velocity of the pebble bed area in the core is considerably smaller when the inlet velocity is 2.98 m/s. Thus, the flow field of the whole core is more uniform except for the slight disturbance near the surface of the lower reflector, as shown in Figs. 7 and 8. According to the calculations and Fig. 8, we can clearly see that the design of the channels with different sizes for the

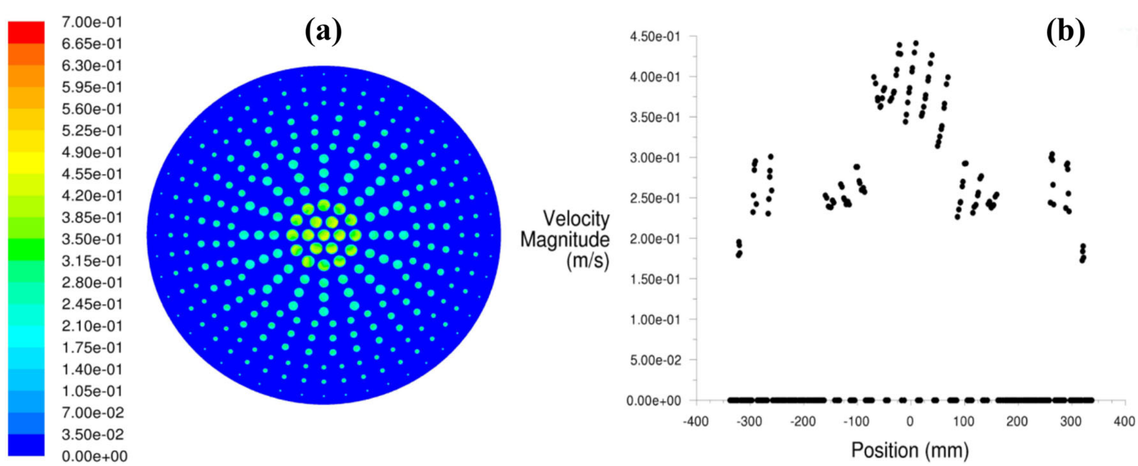

Fig. 9 (Color online) Velocity field of the undersurfaces of channels of the core shroud floor: **a** contours of radial velocity magnitude (m/s) and **b** plots of radial velocity magnitude (m/s)

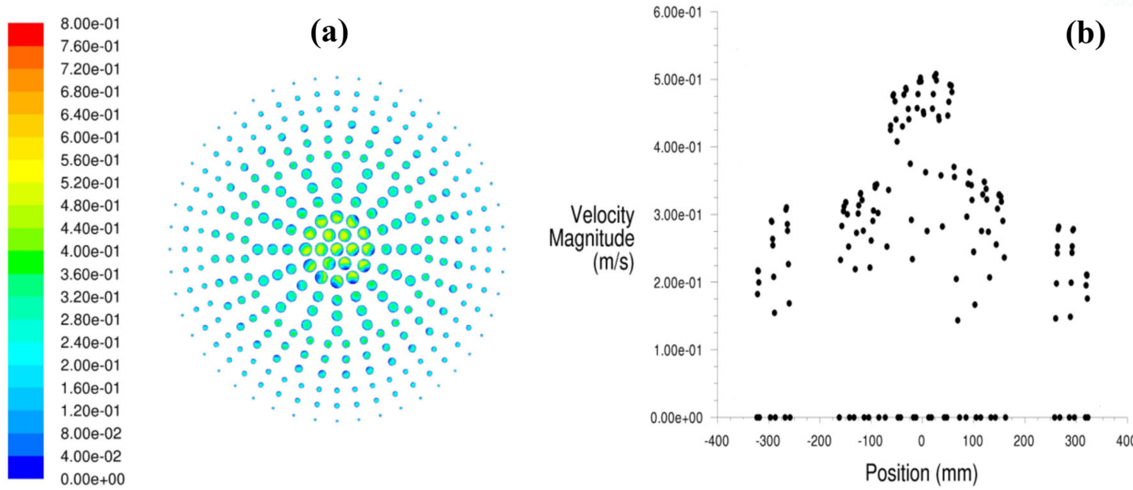

Fig. 10 (Color online) Velocity field of the undersurfaces of channels of the lower reflector: **a** contours of radial velocity magnitude (m/s) and **b** plots of radial velocity magnitude (m/s)

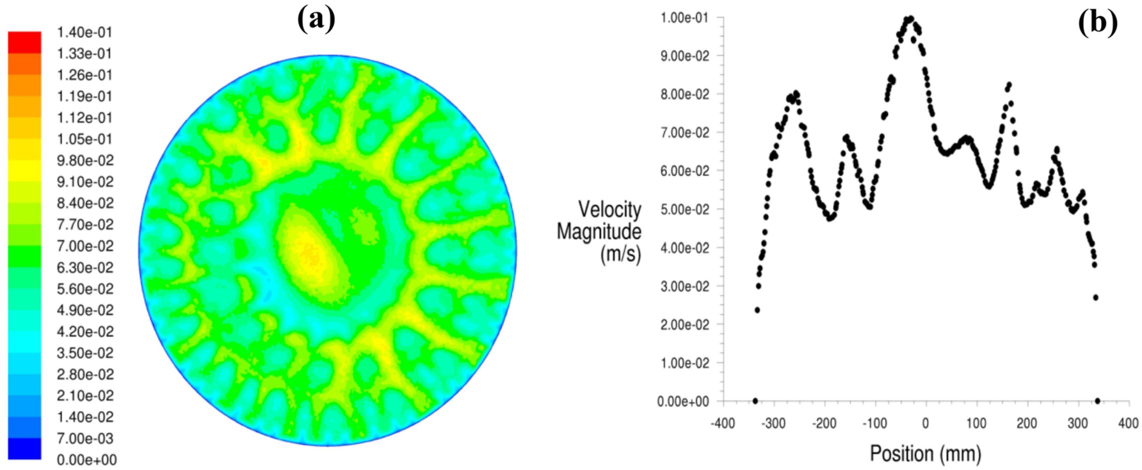

Fig. 11 (Color online) Velocity field at the bottom of the pebble bed of the core: **a** contours of radial velocity magnitude (m/s) and **b** plots of radial velocity magnitude (m/s)

Table 5 Calculations with inlet velocity of 2.98 m/s

Velocity of important fluid domains	Average velocity (m/s)	Maximum velocity (m/s)
Velocity of pebble bed area in the core	0.037	0.037
Entrance velocity of channels of the core shroud floor	0.137	0.457
Entrance velocity of channels of the lower reflector	0.271	0.512
Entrance velocity at the bottom of pebble bed in the core	0.077	0.105

core shroud floor and the design of the lower reflector can effectively reduce the flow velocity and disturbance at the bottom of the pebble bed in the core. From Figs. 9 and 10, it can be clearly seen that the flow velocity in each model becomes larger with the diameter of channels of the core shroud floor and the lower reflector, and the maximum velocity is generated from the middle channels.

From Table 5, it is clearly seen that the average velocity and the maximum velocity at the bottom of the pebble bed in the core are smaller, and therefore, there is almost no big eddies at the bottom of the pebble bed that is shown in Fig. 8. All the simulation results prove the stability of the flow field at the bottom of the pebble bed in the core.

5 Conclusion

The flow field in the core of VEFPB was analyzed by using model simplification and the local mesh encryption method. Results showed that appropriate channel designs of the core shroud floor and the lower reflector are significant for obtaining the flow field at the bottom of pebble bed according to the velocity field of the core, which can obviously reduce the eddies at the bottom of pebble bed in the core. They also showed that the disturbance at the bottom of the pebble bed is proportional to the flow velocity of the inlet pipe, and the flow velocity close to the inlet side is more significant than that in other parts, and the flow field distribution of the core is considerably uniform except at the bottom of the pebble bed.

Simulation results showed that the flow field distribution of the pebble bed in the core is stable overall, except for the small disturbance at the bottom of the pebble bed, and the maximum velocity of the pebble bed in the core is only 0.037 m/s, which can be ignored. Thus, the design of VEFPB is feasible and reasonable, making the pebble bed in the core of VEFPB stable and the flow field uniform and finally meeting experimental requirements.

This study will serve as a reference for the later experiments on VEFPB, for the flow field analysis of the core of TMSR, and for the designs of different experimental devices of TMSR. The rationality of the flow field analysis of VEFPB will further be verified by conducting experiments and comparing the simulation results with the experimental results.

References

1. T. Yamamoto, K. Mitachi, T. Suzuki, Steady state analysis of molten salt reactor in consideration of the effect of fuel salt flow, in *ICONE12-49077*, Vol. 1 (2004), pp. 275–282. https://doi.org/10.1115/icone12-49077
2. M.D. Mei, D.F. Lin, X.W. Chen et al., Flow distribution plate design of molten salt reactor based on pebble bed dense experiment facility. Nucl. Tech. **40**, 040605 (2017). https://doi.org/10.11889/j.0253-3219.2017.hjs.40.040605. **(in Chinese)**
3. C.W. Forsberg, P.F. Peterson, P.S. Pickard et al., Molten-salt-cooled advanced high-temperature reactor for production of hydrogen and electricity. Nucl. Tech. **144**, 289–302 (2003). https://doi.org/10.13182/nt03-1
4. D.Y. Cui, S.P. Xia, X.X. Li et al., Transition toward thorium fuel cycle in a molten salt reactor by using plutonium. Nucl. Sci. Tech. **28**, 152 (2017). https://doi.org/10.1007/s41365-017-0303-y
5. R.O. Scarlat, M.R. Laufer, E.D. Blandford et al., Design and licensing strategies for the fluoride-salt-cooled, high-temperature reactor (FHR) technology. Prog. Nucl. Energy **77**, 406–420 (2014). https://doi.org/10.1016/j.pnucene.2014.07.002
6. J.Y. Lee, S.Y. Lee, Flow visualization in the scaled up pebble bed of high temperature gas-cooled reactor using particle image velocimetry method. J. Eng. Gas Turbines Power **131**, 064502 (2009). https://doi.org/10.1115/1.3098417
7. Y.A. Hassan, E.E. Dominguez-Ontiveros, Flow visualization in a pebble bed reactor experiment using PIV and refractive index matching techniques. Nucl. Eng. Des. **238**, 3080–3085 (2008). https://doi.org/10.1016/j.nucengdes.2008.01.027
8. A. Griveau, Modeling and transient analysis for the pebble bed advanced high temperature reactor ∼ PB-AHTR, Master. Thesis, University of California, Berkeley (2007)
9. D. LeBlanc, Molten salt reactors: a new beginning for an old idea. Nucl. Eng. Des. **240**, 1644–1656 (2010). https://doi.org/10.1016/j.nucengdes.2009.12.033
10. D. Yang, Z. Cao, X.J. Hao et al., Readout electronics of a prototype time-of-flight ion composition analyzer for space plasma. Nucl. Sci. Tech. **29**, 60 (2018). https://doi.org/10.1007/s41365-018-0390-4
11. Z.H. Zhou, D. Pan, Y.S. Chen et al., Core flow distribution design of molten salt reactor with liquid fuel. Nucl. Tech. **39**, 050601 (2016). https://doi.org/10.11889/j.0253-3219.2016.hjs.39.050601. **(in Chinese)**
12. N.N. Zhang, C.Q. Yan, L.C. Sun et al., Numerical simulation on internal flow field in gas separator of molten salt reactor. Atomic Energy Sci. Tech. **48**, 2208–2212 (2014). https://doi.org/10.7538/yzk.2014.48.12.2208. **(in Chinese)**
13. R. Vadi, K. Sepanloo, An improved porous media model for nuclear reactor analysis. Nucl. Sci. Tech. **27**, 24 (2016). https://doi.org/10.1007/s41365-016-0016-7
14. H. Li, S. Qiu, Y. Zhang et al., Thermal hydraulic investigations with different fuel diameters of pebble bed water cooled reactor in CFD simulation. Ann. Nucl. Energy **42**, 135–147 (2012). https://doi.org/10.1016/j.anucene.2011.11.010
15. Y. Liu, O. Hinrichsen, CFD simulation of hydrodynamics and methanation reactions in a fluidized-bed reactor for the production of synthetic natural gas. Ind. Eng. Chem. Res. **53**(22), 9348–9356 (2014). https://doi.org/10.1021/ie500774s
16. M.H. Salhi, S.E.H. Abaidia, B. Mohamedi et al., Cooling enhancement of planar-balanced magnetron cathode. Nucl. Sci. Tech. **28**, 111 (2017). https://doi.org/10.1007/s41365-017-0271-2
17. H.P. Dong, W.Y. Fan, Y. Guo, CFD investigation and optimization on flow distribution of plate-type assembly. Nucl. Tech. **39**, 080603 (2016). https://doi.org/10.11889/j.0253-3219.2016.hjs.39.080603. **(in Chinese)**
18. D. Pavlidis, D. Lathouwers, Fluid flow and heat transfer investigation of pebble bed reactors using mesh-adaptive LES. Nucl. Eng. Des. **264**, 161–167 (2013). https://doi.org/10.1016/j.nucengdes.2013.07.005
19. J.J. Zhou, Z.P. Guo, S.Z. Qiu et al., The influence of lower plenum and distribution plates to thermal hydraulics characteristics of MSR. Nucl. Eng. Des. **256**, 235–248 (2013). https://doi.org/10.1016/j.nucengdes.2012.11.004
20. D. Pan, X.H. Yu, Y. Zou et al., CFD-simulation of structured packed beds molten salt reactors on pressure drop and heat transfer. Nucl. Tech. **39**, 080604 (2016). https://doi.org/10.11889/j.0253-3219.2016.hjs.39.080604. **(in Chinese)**
21. Y.H. Li, W. Ji, Effects of fluid–pebble interactions on mechanics in large-scale pebble-bed reactor cores. Int. J. Multiph. Flow **73**, 118–129 (2015). https://doi.org/10.1016/j.ijmultiphaseflow.2015.03.004
22. F.R. Liu, X.W. Chen, Z. Li et al., DEM-CFD simulation of modular PB-FHR core with two-grid method. Nucl. Sci. Tech. **28**, 100 (2017). https://doi.org/10.1007/s41365-017-0246-3
23. J.H. Chen, H.Q. Zhang, L.S. Lv et al., Numerical simulation study on heat transfer characteristics of new heat exchange fins. Nucl. Tech. **41**, 100601 (2018). https://doi.org/10.11889/j.0253-3219.2018.hjs.41.100601. **(in Chinese)**

24. C.C. Yue, L.L. Chen, K.F. Lyu et al., Flow characteristics of natural circulation in a lead-bismuth eutectic loop. Nucl. Sci. Tech. **28**, 39 (2017). https://doi.org/10.1007/s41365-017-0187-x
25. J.H. Chen, H.Q. Zhang, Z.Y. Zhu et al., Coupled neutronic and thermal-hydraulic analysis of TMSR-SF1 at steady state. Nucl. Tech. **40**, 080603 (2017). https://doi.org/10.11889/j.0253-3219.2017.hjs.40.080603. **(in Chinese)**
26. C. Guo, Y.T. Song, M.Z. Lei et al., Design and thermal-hydraulic analysis of helium cooled solid breeder blanket for CFETR. Nucl. Tech. **41**, 040601 (2018). https://doi.org/10.11889/j.0253-3219.2018.hjs.41.040601. **(in Chinese)**
27. ANSYS, Inc, *ANSYS Fluid Dynamics Verification Manual* (ANSYS, Inc, Canonsburg, 2013)
28. K. Xie, L.S. Li, F.Shen et al., Heat transfer analysis of TMSR core based on porous medium model of ANSYS CFX. At. Energy Sci. Technol. **49**, 294–300 (2015). https://doi.org/10.7538/yzk.2015.49.S0.0294. **(in Chinese)**